DOI: 10.1002/chem.200900301

Synthesis, Stabilization, Functionalization and, DFT Calculations of Gold Nanoparticles in Fluorous Phases (PTFE and Ionic Liquids)

Engelbert Redel,[a] Michael Walter,[b] Ralf Thomann,[b] Christian Vollmer,[a] Laith Hussein,[b] Harald Scherer,[a] Michael Krüger,[b] and Christoph Janiak*[a]

Abstract: Gold nanoparticles (Au-NPs) were reproducibly obtained by thermal, photolytic, or microwave-assisted decomposition/reduction under argon from Au(CO)Cl or $KAuCl_4$ in the presence of *n*-butylimidazol dispersed in the ionic liquids (ILs) $BMIm^+BF_4^-$, $BMIm^+OTf^-$, or $BtMA^+NTf_2^-$ ($BMIm^+$ = *n*-butylmethylimidazolium, $BtMA^+$ = *n*-butyltrimethylammonium, $OTf^- = {}^-O_3SCF_3$, $NTf_2^- = {}^-N(O_2SCF_3)_2$). The ultra small and uniform nanoparticles of about 1–2 nm diameter were produced in $BMIm^+BF_4^-$ and increased in size with the molecular volume of the ionic liquid anion used in $BMIm^+OTf^-$ and $BtMA^+NTf_2^-$. Under argon the Au-NP/IL dispersion is stable without any additional stabilizers or capping molecules. From the ionic liquids, the gold nanoparticles can be functionalized with organic thiol ligands, transferred, and stabilized in different polar and nonpolar organic solvents. Au-NPs can also be brought onto and stabilized by interaction with a polytetrafluoroethylene (PTFE, Teflon) surface. Density functional theory (DFT) calculations favor interactions between IL anions instead of IL cations. This suggests a Au···F interaction and anionic Au_n stabilization in fluorine-containing ILs. The ^{19}F NMR signal in $BMIm^+BF_4^-$ shows a small Au-NP concentration-dependent shift. Characterization of the dispersed and deposited gold nanoparticles was done by transmission electron microscopy (TEM/HRTEM), transmission electron diffraction (TED), dynamic light scattering (DLS), UV/Vis absorbance spectroscopy, scanning electron microscopy (SEM), electron spin resonance (ESR), and electron probe micro analyses (EPM, SEM/EDX).

Keywords: density functional calculations · gold · ionic liquids · nanoparticles · nanotechnology · surface chemistry

Introduction

Gold is a preferred metal in nanotechnology research for most applications that involve colloidal metals.[1] The wealth of size-, shape-, and environment-dependent optical properties of gold nanoparticles[2] contributes to the choice of gold in nanotechnological applications in catalysis, chemical and biological sensors, actuators, optical coatings and electronic devices.[3–6] Colloidal gold has a much longer history than that of any other metal. Systematic research started with Faraday's ground-breaking work in 1857 about colloidal gold solutions which describes the "finely divided metallic state" of gold.[7] The importance of gold in the field of nanoscience and nanotechnology stems from its unique stability as a pure metal.[8] Most other metals are rapidly covered by a passivating oxide film under ambient conditions,[9] which makes them unsuitable for the fabrication of metallic nanostructures, in which the majority of metal atoms are located at the surface. Most colloidal gold or gold nanoparticles syntheses are carried out using the classical Turkevich citrate reduction route[8,10] and its modifications[11,12,24] in common organic solvents. Thus, typically, $HAuCl_4$ is reduced by citric acid which simultaneously functions as a stabilizing agent or is reduced by $NaBH_4$ in the presence of thiol or carboxylic acid stabilizers.

[a] E. Redel, C. Vollmer, Dr. H. Scherer, Prof. Dr. C. Janiak
Institut für Anorganische und Analytische Chemie
Universität Freiburg
Albertstr. 21, 79104 Freiburg (Germany)
E-mail: janiak@uni-freiburg.de

[b] Dr. M. Walter, Dr. R. Thomann, L. Hussein, Dr. M. Krüger
FMF (Freiburger Material Forschungszentrum),
IMTEK (Institut für Mikrosystemtechnik), Universität Freiburg
Stefan-Meier-Str. 21 and Georg Köhler Allee 103, 79104 Freiburg

Supporting information for this article is available on the WWW under http://dx.doi.org/10.1002/chem.200900301. It contains statistical graphs for dynamic light scattering, additional TEM, HRTEM and TED pictures, SEM, EPM, EDX, EPR and NMR spectra of the MNP/IL dispersions and the gold functionalized PTFE (Teflon) surface and DFT calculation pictures.

The controlled and reproducible synthesis of defined and stable metal nanoparticles (M-NPs) is of high importance for various applications.[12–17] Recently, ionic liquids (ILs) were demonstrated as a favorable template for the preparation of predictable chemical nanostructures.[28,38,39,40,54,86] Ionic liquids stabilize metal nanoparticles due to their high ionic charge, high polarity, high dielectric constant and the ability to form supramolecular networks.[18–21] According to the DLVO (Derjaugin–Landau–Verwey–Overbeek) theory,[22,23] which treats the IL ions as point charges, ILs should provide an electrostatic protection in the form of a "protective shell" for M-NPs so that no extra stabilizing molecules or organic solvents are needed.[24–26] Real-life anions with a molecular volume would be classified as electronic and steric or "electrosteric" stabilizers.[27] The stabilization of M-NPs in ionic liquids could, thus, be attributed to "extra-DLVO" forces,[27] involving effects from the network properties of ionic liquids like hydrogen bonding, hydrophobic effects and steric interactions. The IL network contains weakly coordinating cations and anions that bind less strongly and are less deactivating to the metal surface than traditional stabilizers or capping ligands.[27,28,39,40] Metal nanoparticle synthesis in ionic liquids can be carried out through thermal reduction[28–31] or decomposition[32] of metal salts or metal complexes, photochemical[33,34]or electrochemical reduction,[35–37] and recently also by thermal and photochemical decomposition of metal carbonyls.[38–42] In addition, a correlation was found between the molecular volume of the anion in the ionic liquid and the size of the synthesized metal nanoparticles.[28,38,40] Yet, for most applications of metal nanoparticles it is necessary to transfer them from the IL synthesis medium to organic or aqueous solvents or onto surfaces.[3–6] Also, films of metals, alloys or semiconductors can be electrodeposited from ionic liquids.[43]

Here we report the preparation of gold nanoparticles (Au-NPs) by thermal decomposition and reduction of Au(CO)Cl or $KAuCl_4$ in the presence of *n*-butylimidazole in different fluorine-containing ILs. The Au-NPs can then be transferred to polar and nonpolar organic solvents by introducing organic capping molecules or onto a polytetrafluoroethylene (PTFE, Teflon) surface. The binding to and stabilization of Au-NPs with the IL anions is confirmed by DFT calculations and is found to be much stronger than the binding to the cations.

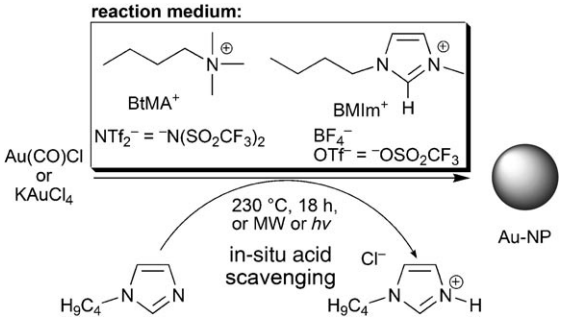

Scheme 1. Formation of Au nanoparticles by thermal decomposition and reduction of different metal precursors in ILs. The formed $HBIm^+Cl^-$ was analyzed by elemental analysis and ^1H NMR spectroscopy.

Results and Discussion

Au-NP syntheses: In a typical experiment, the gold precursor was dissolved in the presence of *n*-butylimidazole under an argon atmosphere in the carefully dried and deoxygenated ionic liquid (IL). The solution was heated under argon to 230 °C for several hours or treated by photolytic (*hν*) or microwave (MW) radiation for some minutes in the ionic liquids *n*-butyltrimethylammonium *N*-bis(trifluoromethylsulfonyl)imide ($BtMA^+NTf_2^-$), *n*-butylmethylimidazolium tetrafluoroborate ($BMIm^+BF_4^-$), or trifluoromethanesulfonate ($BMIm^+OTf^-$) (Scheme 1). The compound Au(CO)Cl[44] starts to decompose at ≈140 °C as evidenced by the gas evolution.

Yellow-orange, red, or red-purple to brown Au-NP dispersions (Figure S45 in the Supporting Information) were reproducibly obtained through decomposition and reduction from their metal precursors in ILs (see Figures 1 and 2 and Table 1). Upon exposure to air, the yellow-orange Au dis-

Table 1. Au-NPs from Au^I and Au^{III} precursors with size and size distribution in different ionic liquids (ILs).

Entry	Ionic liquid[a]	Metal precursor (1 wt% in IL)[a] /decomposition time	TEM & HRTEM median diameter [nm] (standard deviation σ)[b]	DLS median diameter [nm] (standard deviation σ)[c]
1a	$BMIm^+BF_4^-$	Au(CO)Cl/18 h	1.8 (±0.4)	3.6 (±1.3)
1b	$BMIm^+BF_4^-$	Au-NPs from 1a after 2 weeks under Ar	3.0 (±0.9)	–
1c	$BMIm^+BF_4^-$	Au-NPs from 1a after 6 weeks under air	3.6 (±0.6)	7.3 (±1.4)
2	$BMIm^+BF_4^-$	$KAuCl_4$/18 h	1.1 (±0.2)	3.3 (±1.1)
3	$BMIm^+BF_4^-$	Au(CO)Cl/MW 5 min	4.1 (±0.7)	8.0 (±2.2)
4	$BMIm^+BF_4^-$	Au(CO)Cl/*hν* 3 min	61 (±43)	154 (±76)
5	$BMIm^+OTf^-$	Au(CO)Cl/18 h	130 (±40)	280 (±140)
6	$BtMA^+NTf_2^-$	Au(CO)Cl/18 h	350 (±180)	600 (±180)

[a] Solubility of metal carbonyl precursors in $BMIm^+BF_4^-$ is limited to a maximum value of about 1–2 wt%. Anion volumes: BF_4^- 0.073±0.009 nm^3; OTf^- 0.131±0.015 nm^3; NTf_2^- 0.232±0.015 nm^3.[50] [b] Statistical evaluation of the total sample pictures (see also Supporting Information). [c] Hydrodynamic radius, median diameter from the first three measurements at 633 nm. The hydrodynamic radius is roughly 2–3 times the size of the pure kernel cluster. For very small Au NPs (~1 nm) the size of the hydrodynamic radius can even increase to more than 3 times the Au NP radius. The resolution of the DLS instrument is 0.6 nm.

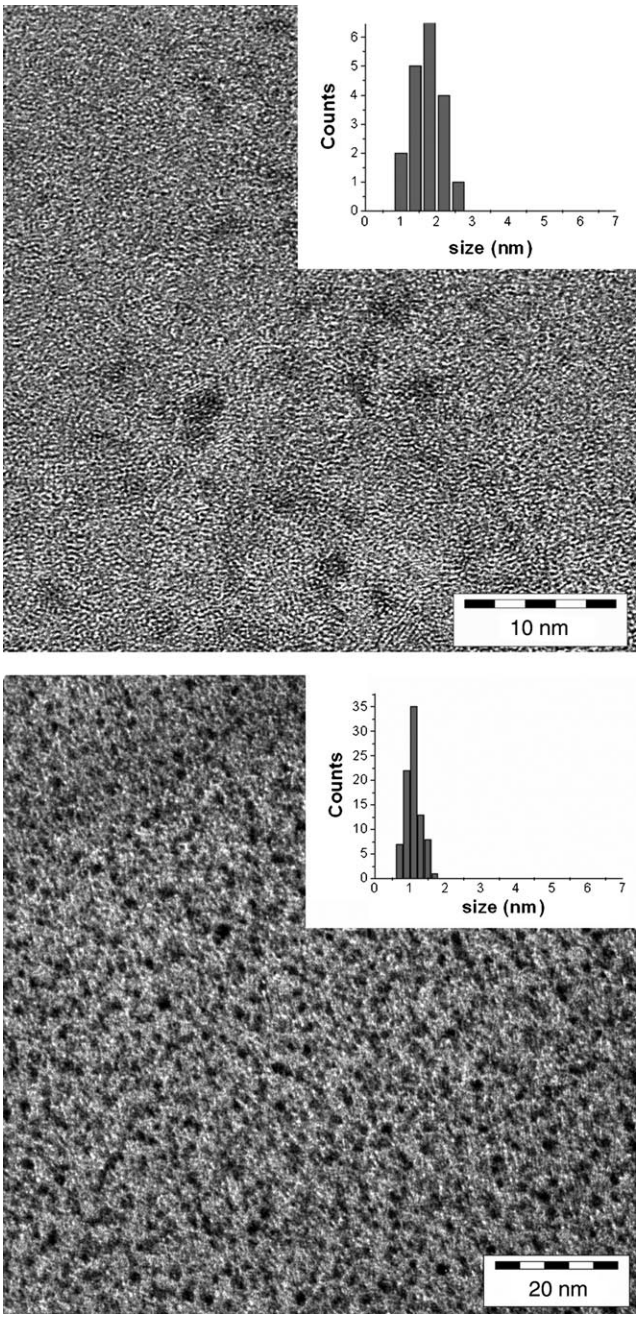

Figure 1. Au-NPs from Au(CO)Cl (HRTEM, top) and from $KAuCl_4$ (TEM, bottom), both in $BMIm^+BF_4^-$ (Table 1, entries 1a and 2).

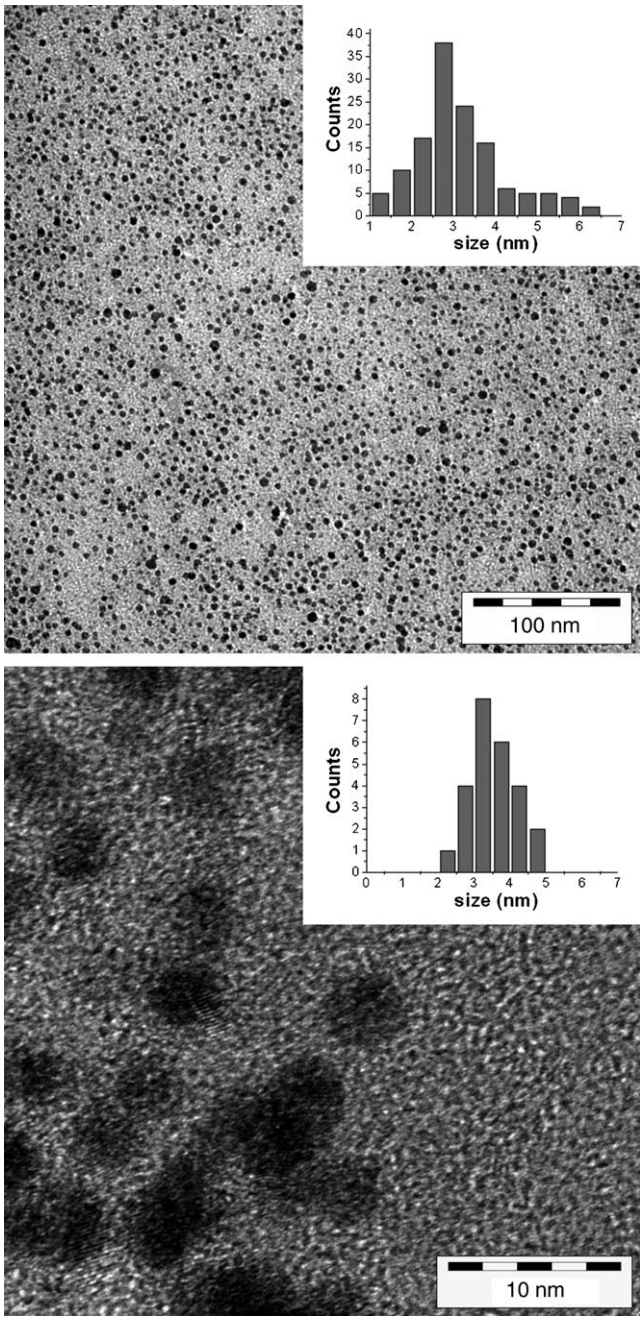

Figure 2. Au-NP precipitate from Au(CO)Cl in $BMIm^+BF_4^-$ after two weeks under argon (TEM, top, Table 1, entry 1b) and after 6 weeks of exposure to air (HRTEM, bottom, Table 1, entry 1c).

persion in $BMIm^+BF_4^-$ forms a red-purple precipitate, indicating particle aggregation (Figure 2). Without the presence of *n*-butylimidazole the Au-NP/IL dispersion also quickly turns red-purple, indicating an agglomeration process which is caused by the generated free HCl acid. As for Pd-NPs, we suggest here the formation of *N*-heterocyclic carbene (NHC)–Au species as the origin of the formation of Au-NPs (Scheme 2).[45,46] We also suggest that the formation of these Au-NHC intermediates slows down the aggregation process. In the presence of *n*-butylimidazole, the released HCl is bound as a new imidazolium salt, similar to the IL matrix.

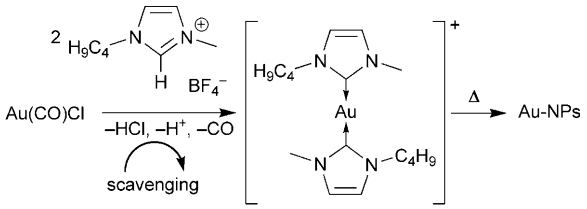

Scheme 2. Suggested Au-NP formation through the formation of an Au–carbene intermediate.[45,46]

This prevents the formation of an acidic reaction medium, which would destabilize the Au-NPs and lead to clustering. The Au-NPs with a size of less than 2 nm are unstable when prepared without a scavenger in ILs. In the absence of the *n*-butylimidazole (BIm) scavenger, the Au-NP size is larger and their size distribution is broader (dynamic light scattering (DLS) ≈4.5 and 15 to 35 nm, Figure S2 in the Supporting Information). This can be reasoned by proton (H^+/HCl) incorporation in the IL dynamic matrix, weakening its stabilizing effect so that larger nanoparticles and size distributions are obtained.[28] In addition, free 1-methylimidazole can stabilize Au-NPs as a ligand in ILs (see DFT calculation).[47]

In $BMIm^+BF_4^-$, the average size of the gold nanoparticles from Au(CO)Cl or $KAuCl_4$ is about 1–2 nm with an extremely small and uniform, albeit not monodisperse, size distribution (Figure 1). Currently, it is not trivial to routinely and easily prepare uniform Au nanoparticles of such small size (1–2 nm). No extra stabilizers or capping molecules are needed to achieve this small particle size. Furthermore, we observed that the ultra small nanoparticles (Table 1) agglomerate in a controlled way by the fusion of two Au-NPs with time and faster when they are exposed to air (Figure 2). Thereby, the particle size doubles (see Figures 1 and 2, entries 1b and c in Table 1) with a still quite uniform size distribution. The use of $BMIm^+OTf^-$ and $BtMA^+NTf_2^-$ as ionic liquids results in much bigger Au nanoparticles with a broad size distribution of about 130 ± 40 and 350 ± 180 nm, respectively (Table 1, Figures S20 and S21 in the Supporting Information), compared to $BMIm^+BF_4^-$. We have previously shown that a larger NP size correlates with a larger volume of the ionic liquid anion.[28,38,40] Agglomeration to larger Au nanoparticles in ionic liquids (ILs) is not prevented, because the interaction of the IL species with the Au-NPs is only weak and is driven by the known strong aurophilic Au–Au interaction (Au cohesive energy 3.8 eV, ≈88 kcal mol^{-1}).[48]

The use of strong heat sources in the microwave or photolytic decomposition (microwave, 10 W, 250 °C or light energy, 1000 W) accelerates the Au-NP agglomeration process in the IL network. Microwave or light energy leads to highly localized "hot spots"[49] through the energy absorption of the Au-NPs.

Such activated particles will be prone to agglomeration. The diffraction patterns from transmission electron diffraction (TED) correspond to the Au metal lattices (Figure 3, Table S1 in the Supporting Information) thereby proving their metal character and the absence of significant oxidation. The crystallinity increases with the size of the Au nanoparticles.[40]

Nanoparticles must be stabilized in order to prevent their agglomeration or aggregation which eventually leads to the formation of small bulk metal particles. Metal nanoparticles (M-NPs, "core") are considered stabilized in ILs by the formation of "protective" anionic and cationic layers ("shells") around them in a "core-shell system".[24,51–54] The first inner shell is believed to be anionic,[22,27,69] because then the IL anion would have the strongest influence on the size and electrostatic stabilization and the anion molecular volume controls the range of the nanoparticle size. In addition, the supramolecular imidazolium-anion clusters of ILs should be taken into account.[28,38,40] Pure ILs can be considered as supramolecular polymeric structures with a high degree of self-organization and weak interactions in an extended network of cations and anions connected together by hydrogen

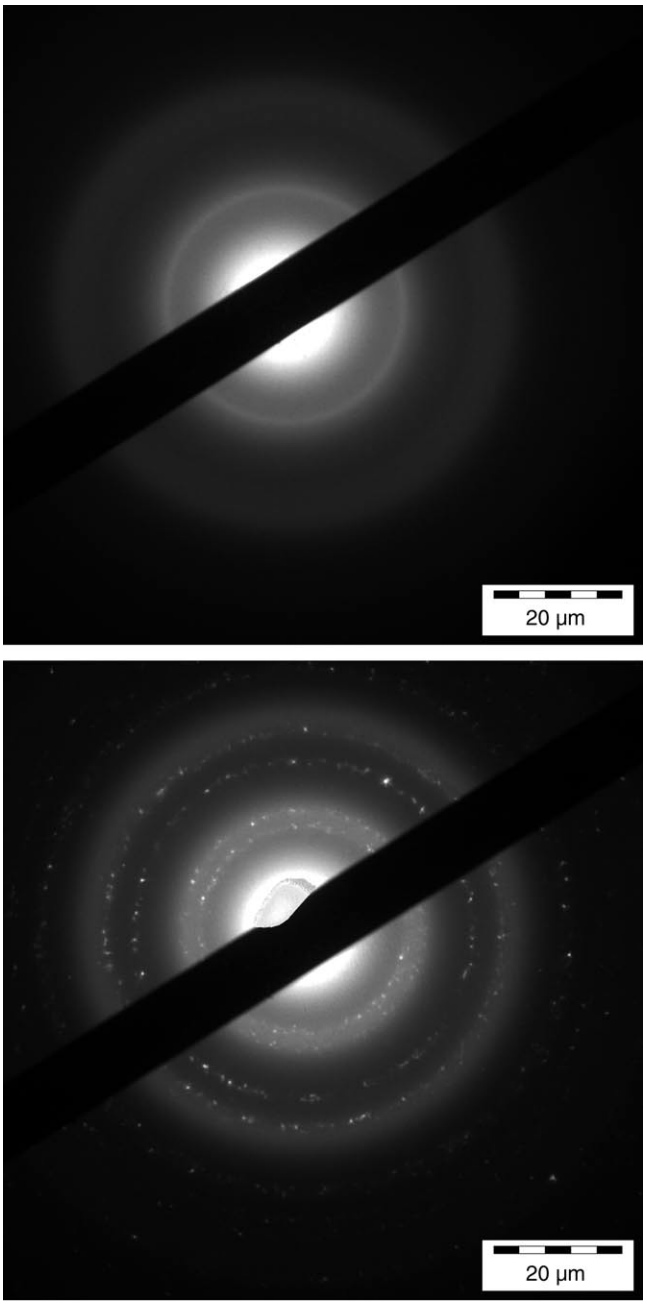

Figure 3. TED picture of 1–2 nm Au nanoparticles from Au(CO)Cl in $BMIm^+BF_4^-$ (top, Table 1, entry 1a), larger Au nanoparticles from Au(CO)Cl in $BMIm^+OTf^-$ (bottom, Table 1, entry 5). The black bar is the beam stopper. The diffraction rings in the right picture at 2.36 (very strong), 2.09 (strong), 1.48, 1.23 (strong), and 0.96 Å (median) match with the *d*-spacing of the Au-metal diffraction pattern (Table S1 in the Supporting Information).[61]

bonds.[19–21] When mixed with other molecules or M-NPs, ionic liquids become nanostructured materials with polar and nonpolar regions.[19–21,55–58] The ionic liquid represents an excellent dynamic nano-environment for the formation of M-NPs with, in most cases, a small size and a narrow size distribution under mild reaction conditions.[28,38,40] We suggest that weak gold–fluorine (Au···F) interactions from the IL anion to the Au nanoparticles may aid in the stabilization (see DFT calculation). Also, such fluorous anion interactions (M···F, M = electrophilic transition metals) in ionic liquids are not limited to Au nanoparticles.

Au-NP surface functionalization: The addition of an organic ligand to the bare M-NP surface is generally described as a surface functionalization, albeit derivatization, coating, or capping maybe better terms. The post synthetic introduction of an organic capping ligand on the dispersed gold nanoparticles in ILs was done by treating the gold dispersion with an excess of mercaptopropionic acid (HS–$(CH_2)_2$–COOH), thioglycolic acid (HS–CH_2–COOH), *n*-decanethiol (HS–$C_{10}H_{21}$), *n*-dodecanethiol (HS–$C_{12}H_{25}$), and *n*-tetradecanethiol (HS–$C_{14}H_{29}$) at room temperature (Scheme 3, Table 2). The strong affinity between the thiol (–SH) group and the gold nanoparticles replaces the ionic liquid protective layer.

Surface capping of gold nanoparticles dispersed in the ionic liquid $BMIm^+BF_4^-$ with a polar and soluble organic thiol ligand leads to slightly larger thiol-capped gold nanoparticles (Figure 4 and Table 2, entries 1–2). The use of a nonpolar and insoluble organic thiol ligand more than doubles the size of the resulting thiol-capped gold nanoparticles (Figure 5 and Table 2, entries 3–5). The aggregation is a result of the introduction of the thiol ligands into the IL network, which disrupts the hydrogen-bonding network. Therefore, the stabilizing properties of the IL network towards the Au-NPs is weakened and results in further Au-NP agglomeration which is driven by the aurophilic Au–Au interaction (Figures 4 and 5 and Table 2).

The interaction with the thiol ligand results in a strong Au–S chemisorption bond.[59] The addition of a thiol ligand leads to larger Au-NPs based on a controlled aggregation of the gold nanoparticles. The larger Au/thiol-covered nanoparticles could be collected by centrifugation. The IL together with the excess thiol ligand is decanted and the Au/thiol-

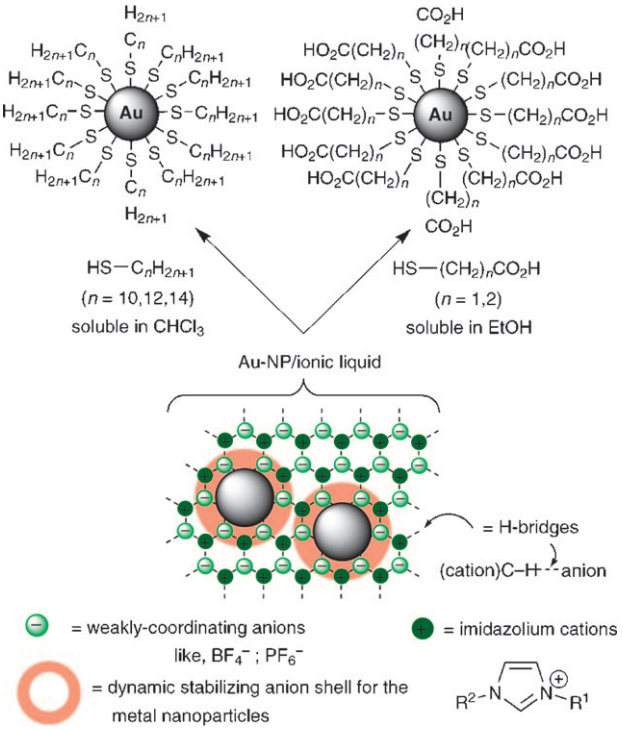

Scheme 3. Stabilization and surface capping (functionalization, derivatization) of Au nanoparticles from the ionic liquid network by hydrophobic and hydrophilic thiols ligands.

NPs were washed twice with a water-methanol solution followed by methanol.[60] The thiol-capped Au nanoparticles can then be re-dispersed in polar or nonpolar organic solvents like ethanol or chloroform (Figures 4 and 5).

The thiol-capped Au/SR-NP (SR = thiol) dispersions in ethanol and $CHCl_3$ are stable for months. The particle size does not change over time, even in air (Figures S9–S13 in the Supporting Information). TED studies show that the thiol-capped Au nanoparticles are not oxidized. The diffraction patterns from TED correspond to their metal lattices (Figure S22 and Table S1 in the Supporting Information),[61] thereby proving their metallic character and the absence of significant oxidation.

Thiolation replaces the weakly bound $BMIm^+BF_4^-$ coating from the dispersed Au-NPs, thereby leading to a struc-

Table 2. Thiol-capped Au/SR-NP from $BMIm^+BF_4^-$ with size distribution in ethanol and chloroform.

Entry	Organic solvent[a]	Thiol ligand	Au-NP original size HRTEM	TEM & HRTEM median diameter [nm] (standard deviation σ)[a]	DLS median diameter [nm] (standard deviation σ)[b]
1	Ethanol	HS–CH_2–COOH	1.8 (±0.4)	2.0 (±0.4)	5.77 (±1.06)[c]
2	Ethanol	HS–$(CH_2)_2$–COOH	1.8 (±0.4)	–	6.97 (±1.25)[d]
3	$CHCl_3$	HS–$(CH_2)_9$–CH_3	1.8 (±0.4)	4.3 (±1)	9.53 (±3.07)
4	$CHCl_3$	HS–$(CH_2)_{11}$–CH_3	1.8 (±0.4)	–	10.2 (±2.81)
5	$CHCl_3$	HS–$(CH_2)_{13}$–CH_3	1.8 (±0.4)	–	11.3 (±2.95)

[a] Statistical evaluation of the total sample pictures (see Supporting Information). TEM and HRTEM show only the Au core cluster. [b] Hydrodynamic radius, median diameter from the first three measurements at 633 nm. The hydrodynamic radius is roughly 2–3 times the size of the Au core cluster due to the ligand and solvent shell. For very small Au-NPs (≈1 nm) the size of the hydrodynamic radius can even increase to more than three times the Au-NP radius. The resolution of the DLS instrument is 0.6 nm. [c] Hydrogen-bonded agglomerates appear in the range of about ≈35 nm. [d] Hydrogen-bonded agglomerates appear in the range of about ≈24 nm.

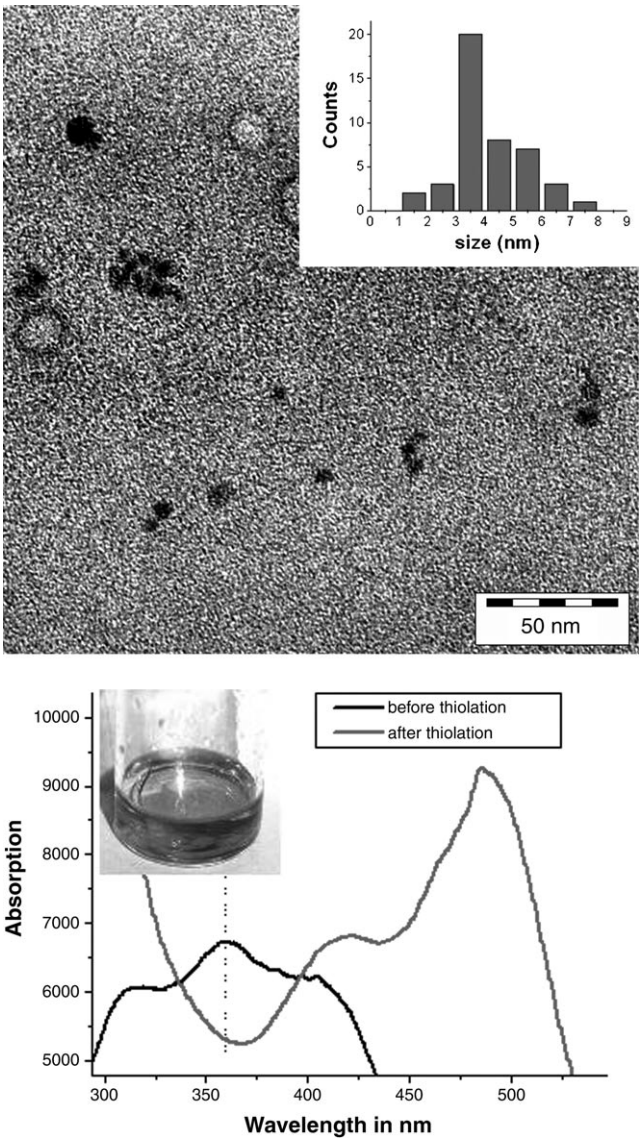

Figure 4. Au/SR-NPs from $BMIm^+BF_4^-$ after thiolation with decanethiol, centrifugation and re-dispersion in $CHCl_3$ TEM picture (top) and UV/Vis spectrum (bottom, grey curve). The black curve is the UV/Vis spectrum of Au-NP/IL(for the colour version see Figure S46 in the Supporting Information).

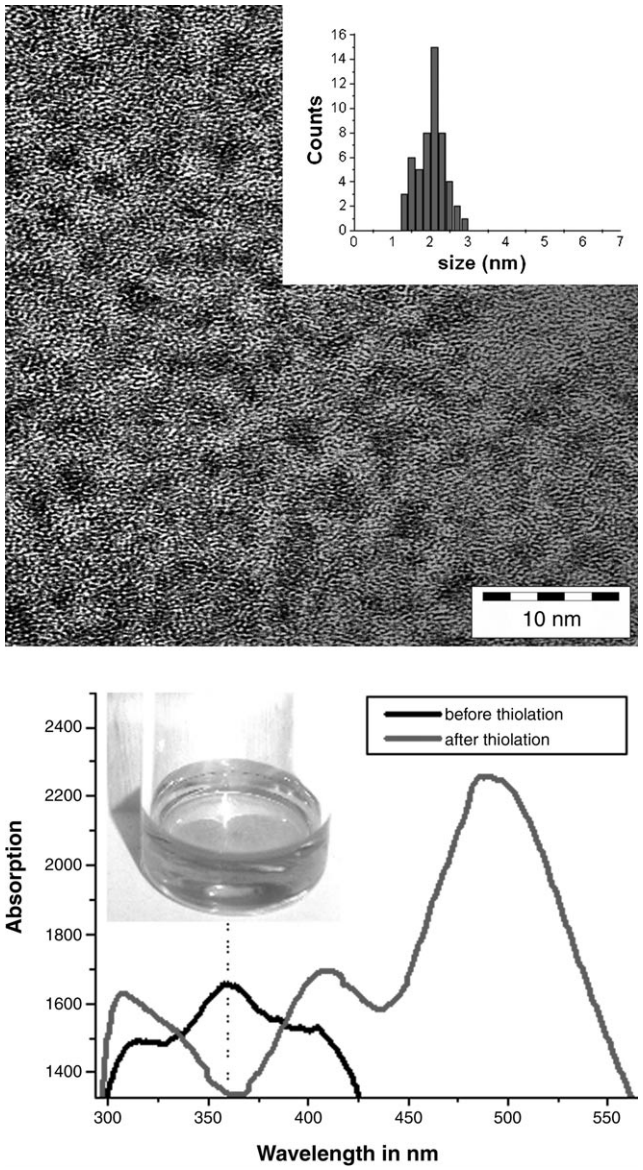

Figure 5. Au/SR-NPs from $BMIm^+BF_4^-$ after thiolation with mercaptopropionic acid, centrifugation and re-dispersion in ethanol HRTEM picture (top) and UV/Vis spectrum (bottom, grey curve). The black curve is the UV/Vis spectrum of Au-NP/IL (for the colour version see Figure S47 in the Supporting Information).

tural organization of the Au clusters and to a controlled agglomeration process[62] (compare Figures 1, 4 and 5, Table 2). Therefore, the process of thiol capping of gold nanoparticles in ionic liquids is similar to a ligand exchange process. It is already known that the exchange of the stabilizers or capping molecules from the nanoparticles surface results in clustering of different, defined gold species, for example from phosphane- or chloride-stabilized Au_{11} to thiol-stabilized Au_{25}[63] and other size changes.[64] In particular, for small clusters, this can be understood due to the strong correlation of specific stable cluster sizes to the nature of a given ligand.[65,66]

Au-NP deposition on PTFE (Teflon): Au-NPs can also be deposited onto and stabilized by interaction with a polytetrafluoroethylene (PTFE, Teflon) surface. The in situ deposition of gold nanoparticles on PTFE was performed using a $10 \times 10\,mm^2$ PTFE sheet or membrane during the Au-NP synthesis and by post-synthetic photolytic treatment from an Au-NP/$BMIm^+BF_4^-$ dispersion (Scheme 4). A controlled deposition of gold nanoparticles onto PTFE (Teflon) could be a great advantage for different applications, for example for the development of electronic, catalytic, and sensor devices.[3,24,48] We chose PTFE as a support material because of its high thermal stability. A sheet made of polypropylene or of poly(difluoroethylene) $(CHF–CHF)_n$ was found to melt quickly at our reaction temperature of about 250 °C. The deposition of Au nanoparticles on PTFE was analyzed with an electron probe micro analyzer (EPM), that, is by scan-

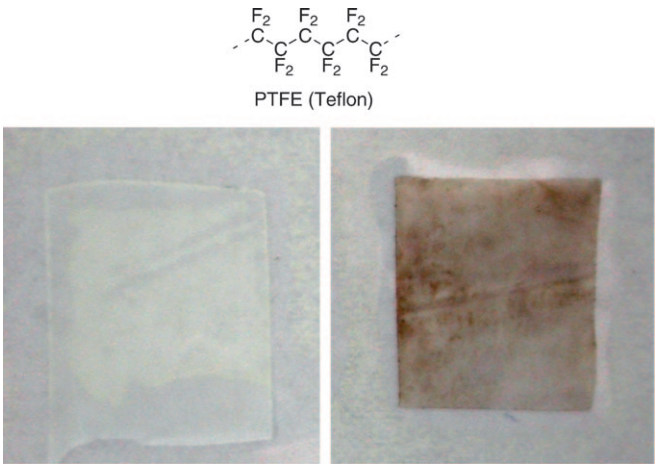

Scheme 4. Surface deposition of Au nanoparticles from $BMIm^+BF_4^-$ on a PTFE surface; photograph of a PTFE sheet before (left) and after (right) the Au-NP deposition

ning electron microscopy (SEM) and energy dispersive X-ray spectroscopy (EDX, Figure 6). Au-NP deposition on PTFE was obtained reproducibly during the nanoparticle synthesis (in situ) by thermal, photolytic, or microwave decomposition/reduction under argon from Au(CO)Cl in the presence of PTFE (Figure 6, bottom left). In addition, Au-NP deposition could be achieved through ultraviolet (UV) irradiation of Au-NP/$BMIm^+BF_4^-$ dispersions in the presence of PTFE (Figure 6, bottom right).

The PTFE sheet or membrane swells in solvents and also in the ionic liquid $BMIm^+BF_4^-$, which leads to a surface change of the PTFE (Figure 6 top left and Figure S24 in the Supporting Information). This swelling contributes to the deposition of the metal nanoparticles. The Au-NPs deposited on the PTFE surface are protected by a thin film of the ionic liquid $BMIm^+BF_4^-$ which could also be detected by the EPM measurements (Figure S31 in the Supporting Information).

The best results for gold deposition on PTFE were obtained by the in situ photolytic and microwave-assisted decomposition reactions of Au(CO)Cl in $BMIm^+BF_4^-$ (Fig-

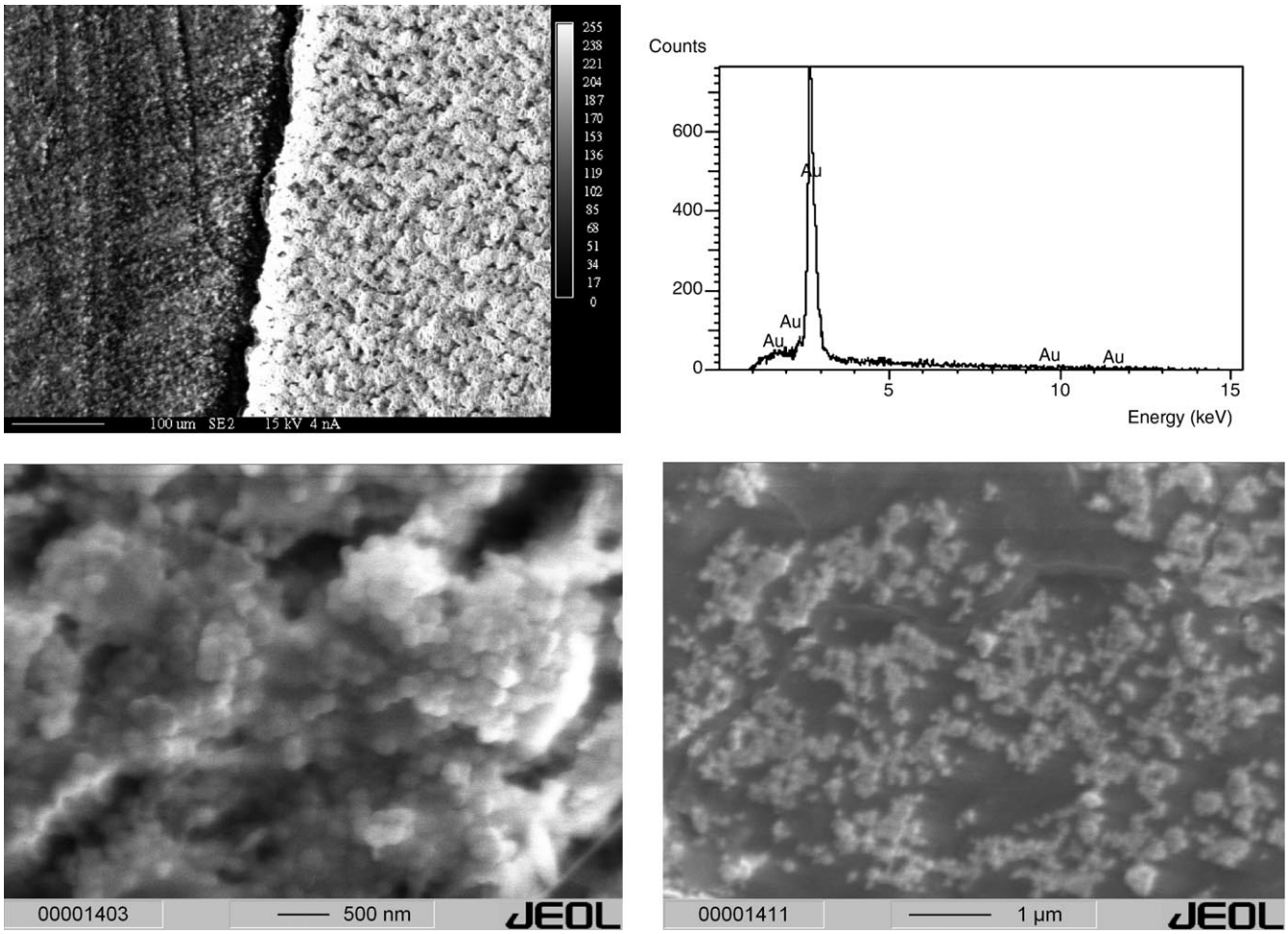

Figure 6. Top left: EPM-SEM picture of PTFE (Teflon) blank (left) and its swelling in the presence of $BMIm^+BF_4^-$ (right). Top right: EDX of Au-NP deposited on the PTFE surface. Bottom left: SEM of Au-NPs on the PTFE membrane through in situ photolytic deposition from Au(CO)Cl in $BMIm^+BF_4^-$. Bottom right: SEM of Au-NPs deposited on the PTFE sheet through UV irradiation from a Au-NP/$BMIm^+BF_4^-$ dispersion.

ures 6, bottom, and Figures S29 and S30 in the Supporting Information). The in situ photolytic deposition on PTFE from Au(CO)Cl/BMIm$^+$BF$_4^-$ results in a high loading of large spherical Au-NPs with a narrow particle size distribution, in comparison to the two other methods, in the range from 170 to 230 nm (Figure 6, bottom left). In situ deposition on PTFE from Au(CO)Cl/BMIm$^+$BF$_4^-$ under microwave conditions gives larger Au-NPs with a broader particle size range from 160 to 1030 nm (Figure S27 and S28 in the Supporting Information). Thermal assisted deposition on PTFE by the decomposition/reduction of Au(CO)Cl results in a lower loading of large particles with a broad particle size distribution in the range from 220 to 1020 nm (Figure S25 and S26 in the Supporting Information). The photolytic deposition on PTFE with pre-synthesized Au-NPs in BMIm$^+$BF$_4^-$ yields Au-NPs with a particle size distribution in the range from 60 to 170 nm (Figure 6, bottom right). Furthermore, in all of the gold deposited samples, EDX studies show that the Au nanoparticles consist only of gold without chlorine atoms (Figure 6, top right).

The Au-NP deposited on PTFE shows an EPR resonances with $g_{iso}=2.126$ and 1.979 (Figure S32 in the Supporting Information). Bulk Au, Au-NP/IL dispersions, PTFE and the ionic liquid are EPR silent. We suggest that the Au particles assume in part a paramagnetic behavior through a charge transfer to the PTFE surface. Possibly localized holes may be generated in the Au 5d shell from a charge transfer to the PTFE surface, similar to that which occurs with S atoms of thiol ligands in forming the Au–S bonds.[67]

NMR studies: The contact of gold nanoparticles with the ionic liquid dynamic matrix was studied by solution NMR (^{19}F, ^{11}B, ^{1}H) spectroscopy. The ^{19}F NMR signals of BMIm$^+$BF$_4^-$ show a small shift if Au-NPs are dispersed in this solvent. The shift increases with the Au-NP concentration, up to 0.02 ppm downfield of the corresponding signal of the pure ionic liquid with about 1 wt.% Au in solution (Figure S33 in the Supporting Information). At the same time, the ^{11}B chemical shift of the anion and the ^{1}H chemical shift of the imidazolium cation remain unchanged (Figures S34 and S35 in the Supporting Information). Due to the weak Au···F contacts, fluctuations and diffusion will lead to a fast exchange between BF$_4^-$ in the vicinity of Au nanoclusters and the bulk ionic liquid. So, on the NMR timescale, different resonances cannot be observed, but a small effect on the chemical shift of the average signal is seen. Although the shift difference is quite small for ^{19}F NMR chemical shifts, the absence of changes in the boron and hydrogen chemical shift makes it unlikely that the shift difference observed in ^{19}F NMR is due to the modification of the overall magnetic susceptibility of the sample by the Au nanoclusters in solution. Thus, this finding supports the idea that there are contacts between the fluorine atoms of the BF$_4^-$ ions and the surface of the gold nanoparticles.

These observations contribute to the model which predicts the anions as the primary source of stabilization for electrophilic metal nanoclusters.[22,27,68] Our NMR studies also agree with the location of PF$_6^-$ ions from BMIm$^+$PF$_6^-$ on a Pd nanocluster surface by X-ray photoelectron spectroscopy (XPS).[68] Moreover, the DFT calculations presented in the next section support the suggested Au-NP···F–BF$_3^-$ interactions, which are crucial for the dynamic IL stabilization of the Au-NPs.

DFT calculations: In IL dispersions, the metal nanoparticles are believed to be surrounded by the anions from the ionic liquid that induce a positive charge on the metal surface.[69] The origin of this model is the DLVO theory in analogy of the charge stabilization of colloids in the presence of anions in common solvents.[22,27,70] On the other hand, a stabilization due to special end groups of the cations has also been proposed.[71] We have investigated the binding of the IL anions and cations, as well as chloride (as a synthetic byproduct from Au(CO)Cl or KAuCl$_4$ or a possible IL impurity) and free imidazoles using density functional theory (DFT) calculations. The exchange-correlation energy was approximated as proposed by Perdew, Burke and Ernzerhof (PBE).[72] The projector augmented wave method[73] was used and the smooth wave functions were represented on uniform real space grids.[74] This approach provides a single convergence parameter, the grid-spacing, to control the accuracy of discretization. Similar techniques have been successfully applied to gold clusters in interaction with organic molecules[64,65,75,76] and ionic metal oxide surfaces.[77,78] The calculations were carefully tested for numerical convergence and found to converge at a grid-spacing of 0.18 Å.

In the following we studied the binding energy (BE) of different IL ions, free bases, and the Cl$^-$ ion to gold clusters of various sizes. The gold clusters considered here are clusters that are known to form in gas phase in their neutral state, a single atom, a dimer, a triangular trimer,[79] triangular Au$_6$,[80] and tetrahedral Au$_{19}$ and Au$_{20}$.[81] The adducts of clusters connected to the ions or free bases were relaxed in the gas phase until the forces fell below 0.05 eV Å^{-1}. Various starting configurations were tried. Generally the binding to the gold cluster corners or edges was found to lead to the largest binding energy due to the enhanced reactivity at these positions.[82] The lowest binding energy configurations were independent of the cluster size and are shown in Figures 7 and 8 for the case of Au$_6$. (See Figures S40–S44 in the Supporting Information for all structurally relaxed energetic minimum configurations.) The BE is defined as the difference of the relaxed energies of the gas-phase anions and the Au$_n$ clusters to the energy of their complex [Eq. (1)].

$$\mathrm{BE} = E(\mathrm{anion}) + E(\mathrm{Au}_n) - E(\mathrm{anion/Au}_n\ \mathrm{complex}) \qquad (1)$$

Figure 7 shows the Au$_n$–anion binding configurations and the variation of the BE with cluster size n. The OTf$^-$ ion binds preferably through an O atom and the fluorous ions through the F atoms. The energy difference for bonding between just one, two, or three F atoms to the gold cluster is found to be isoenergetic (energy difference <0.1 eV). All the anions show a similar behavior in their BEs. The BE to

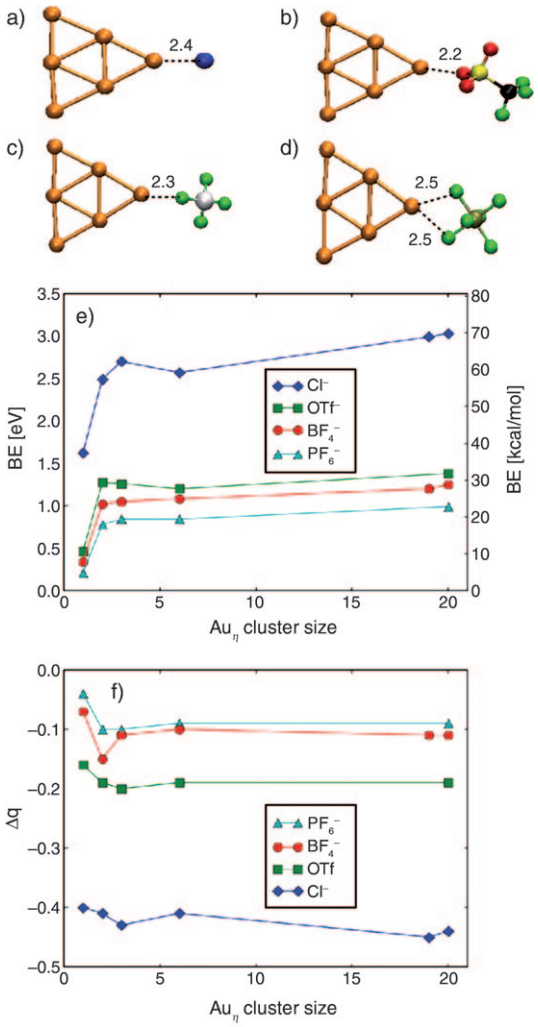

Figure 7. Relaxed configurations of Au_6 bound to a) Cl^-, b) OTf^-, c) BF_4^- and d) PF_6^-. The bond lengths are given in Å. e) Binding energy and f) charge transfer to the gold clusters Δq in $|e|$ for different anions depending on the Au_n cluster size.

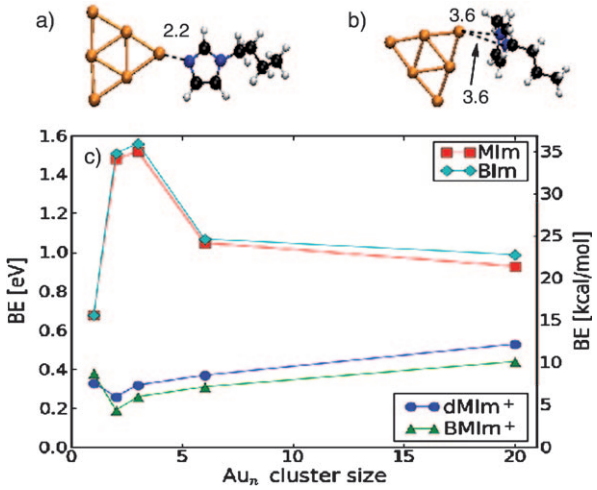

Figure 8. Relaxed configurations of Au_6 bound to a) BIm and b) $BMIm^+$. The distances of the N atoms to the nearest Au atom are given in Å. c) Binding energy of the bases MIm, BIm and the $dMIm^+$ and $BMIm^+$ ions depending on the Au_n cluster size.

a single gold atom $n=1$ is quite low and more than doubles for Au_2 ($n=2$). Increasing the cluster size to $n=20$ does not change the BE substantially any further, in other words, the BE is already saturated for Au_2 (Figure 7). This behavior is reflected in the bond length between gold clusters and anions depending on the cluster size as shown in Figure S37 of the Supporting Information. Similar behavior can be observed for chloride ions, which are present as a synthetic by-product from Au(CO)Cl or $KAuCl_4$ and as a contaminant from the IL synthesis process. Remarkably, the chloride ion shows the largest BE of all anions and can, hence, be expected to be bound to the clusters if it is present in the dispersion. The interaction between anions and gold clusters is accompanied by the considerable charge transfer from the anions to the gold. The strength of the interaction is related to the charge transferred and inversely related to the calculated vertical electron detachment energies (electron affinities) of 3.58, 4.96, 6.39, and 6.76 eV for Cl, OTf, BF_4 and PF_6, respectively. The variation of the charge transfer with cluster size is rather small compared to the strong variation of the corresponding gold cluster electron affinities.[83] This confirms the saturation effect already seen in BE and bond length.

An explanation for the difference in the BE of a single Au atom and the saturation of the binding energy for $n \geq 2$ is found in the local density of states (LDOS) shown in Figure 9 for the representative examples of BF_4^- bound to Au and BF_4^- bound to Au_2. In the case of a single gold atom attached to the BF_4^- ion, the LDOS of both fragments

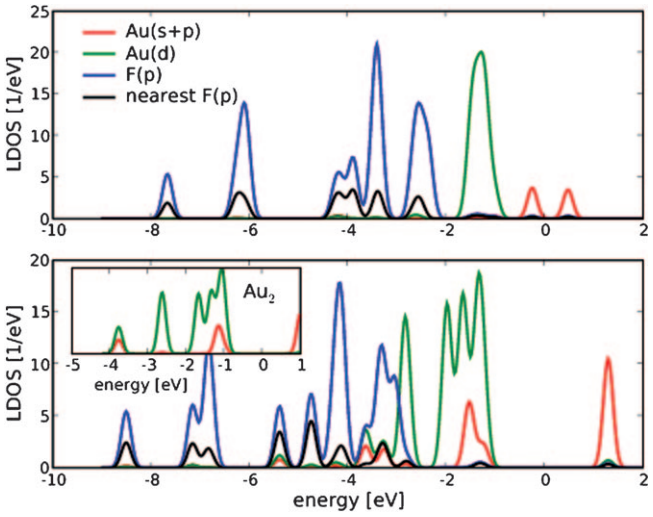

Figure 9. The spin averaged local density of electronic states (LDOS) of Au (top) and Au_2 (bottom) bound to BF_4^-. The inset in the bottom part shows the LDOS of gas phase Au_2. The LDOS of the F atom nearest to gold is shown in black, and the contribution of all F atoms is shown in blue. The Fermi energy was set to 0 eV, and the density of electronic states was folded with Gaussians of 0.1 eV width.

are well separated in energy and the gold d band is located in a narrow energy range (Figure 9a). The slight broadening of the d band can be attributed to spin splitting and a polarization effect due to the neighborhood of the charged BF_4^- ion. In contrast to this, the LDOS of BF_4^- and Au_2 show a clear overlap in the energy region between −4 and −3 eV (Figure 9b). This effect is strongest for the F atom nearest to gold. Here, the states are simultaneously located on the anion as well as on the gold dimer Au_2 by a signature of a weak covalent binding interaction in our gas-phase approximation. Comparison with the LDOS of gas phase Au_2 shows that the overlap is significant only for the gold s and p contributions, and the gold d band is not greatly affected. This covalent character of the anion–gold interaction explains the saturation of the BE with increasing cluster size. In particular, for the case of the chloride anion, this finding is consistent with the strong covalent binding of chloride ions to the Au(111) surface found in recent DFT simulations.[84]

In contrast to the case of the anions, the BEs of the $BMIm^+$ and dimethylimidazolium ($dMIm^+$) ions are much lower than the BE of the anions (< 0.5 eV), Figure 8c). This is reflected in the much larger distance between the cation and the gold cluster (Figure 8b). With the exception of a slight decrease from Au to Au_2, the cationic BE is found to steadily increase with increasing cluster size. This is an indication that the binding in this case is not covalent but polar. The free imidazole bases methylimidazole (MIm) and *n*-butylimidazole (BIm), however, show binding energies similar to the anions, both in strength as well as in cluster size dependence (Figure 8c). This supports the model of stabilization enhancement due to free bases which has been recently proposed.[47]

Conclusions

Gold nanoparticles (Au-NPs) can reproducibly be obtained by thermally, including microwaves, or photolytically induced reduction of their metal carbonyl Au(CO)Cl or $KAuCl_4$ salt in different ionic liquids (ILs). Au nanoparticles synthesized in $BMIm^+BF_4^-$ are very small with a uniform size of about 1–2 nm. No extra stabilizers or capping molecules are needed to achieve such small particle sizes. The Au-NP size increases with the size of the IL anion, from BF_4^- to OTf^- to NTf_2^-. The ILs act as a template for the preparation of predictable chemical nanostructures and their subsequent coating or deposition. From the IL dispersion, the Au-NPs could be coated with different organic thiol ligands and transferred to polar and nonpolar organic solvents. A controlled particle agglomeration, leading to a doubling of the Au/SR-NPs, was observed during the thiolation reaction. Furthermore, Au-NPs could be deposited onto a PTFE surface either during their synthesis (in situ) or through a post-synthetic UV irradiation of Au-NP/$BMIM^+BF_4^-$ dispersions in the presence of PTFE. A small and Au concentration-dependent ^{19}F NMR chemical-shift difference (not seen in ^{11}B or ^1H NMR) for Au-NP/$BMIM^+BF_4^-$ supports the notion of a BF_4^- F···Au-NP contact. DFT calculations in a gas phase model further support IL anion···Au-NP interactions, which are crucial for the NP stabilization in dynamic ILs. The calculations indicate a weak covalent part in this interaction. Free imidazole bases (such as 1-methylimidazole) show similar BE and dependence on cluster size. The Cl^- ions are found to have the highest binding energy and can therefore be expected to bind to the NP if present in the solution. Moreover, significant binding of the $BMIm^+$ or MIm^+ ions was not found. These findings support the model of preferred interaction between anions and Au-NPs, but also confirm the importance to consider a possible presence of Cl^- ions in the ionic liquid solution. Furthermore, we suggest that these fluorine containing anion-to-metal (F···M) interactions in ionic liquids are not limited to Au nanoparticles but extend to all electrophilic transition metals.

Experimental Section

Materials and instrumentation: Au(CO)Cl and $KAuCl_4$ were obtained from STREM, *n*-butylimidazole (p.a.) was obtained from Aldrich, the ionic liquids (ILs) *n*-butyltrimethylammonium bis(trifluoromethylsulfonyl)imide ($BtMA^+NTf_2^-$), *n*-butylmethylimidazolium tetrafluoroborate ($BMIm^+BF_4^-$), and trifluoromethanesulfonate ($BMIM^+OTf^-$) from IoLiTec (H_2O content ≪100 ppm; Cl^- content ≪50 ppm). PTFE membranes cut to 10×10 mm^2 per piece from the 45 mm diameter commercially obtained membranes from Sartorius Stedim Biotech GmbH, 65 μm thickness, pore size 0.45 μm; PTFE pieces cut to 10×10 mm^2 sections from PTFE sleeves intended for NS 29 glass joints, 0.05 mm thickness from VWR International GmbH.

All manipulations were done by using Schlenk techniques under argon since the Au(CO)Cl is hygroscopic and air sensitive. The ionic liquids were dried under a high vacuum (10^{-3} mbar) for several days to avoid, especially in the case of $BMIm^+BF_4^-$, hydrolysis to HF.[85–88]

Transmission electron microscopy (TEM and TED) and high resolution transmission electron microscopy (HRTEM) photographs were taken at room temperature from a carbon-coated copper grid by a Zeiss LEO 912 (TEM) transmission electron microscope operating at an accelerating voltage of 120 kV and on a HRTEM Phillips CEM 200 ST high resolution transmission electron microscope operating at an accelerating voltage of 200 kV. UV/Vis absorption measurements on Au-NP dispersions were done with a J&M TIDAS UV/Vis spectrometer in the wavelength range between 300 and 800 nm. Scanning electron microscopy (SEM) photographs were taken at room temperature from a JOEL JSM-6300F scanning microscope operating at an accelerating voltage of 5 kV. Energy dispersive spectrometry (EDS) measurements were performed on a CAMECA SX100, electron probe micro analyzer (EPMA) equipped with an Oxford Penta FET detector, at room temperature with an accelerating voltage of 15 kV. A Malvern Zetasizer Nano-ZS was used for the dynamic light scattering measurements working at a wavelength of 633 nm. Care was taken for choosing the right parameters, such as the index of refraction of Au (2.4) with an absorption of 0.1 at this wavelength. Samples were prepared by dilution of the metal/IL dispersion (10 μL; 1 wt.% of Au) in *n*-butylimidazole (2 mL, 99% p.a.; particle free). Then, the Au/IL/*n*-butylimidazole solution (150 μL) was diluted further with *n*-butylimidazole (1.5 mL) and was placed in a glass cuvette before measurement.

NMR experiments were carried out on a BRUKER AVANCE II WB spectrometer with a 5 mm ATM-BBFO probe head at room temperature. The spectrometer was locked and shimmed on a sample containing a mixture of $BMIm^+BF_4^-$ and $CDCl_3$. The subsequent samples were measured without locking. To avoid field shifts by shim gradients, these sam-

ples were not further shimmed. The field drift of the magnet was 0.5 Hz per hour. Electron spin resonances (ESR) measurements were measured on an ESP 300E at room temperature in glass tube under continuous wave (CW) conditions.

The quantitative analysis of the gold content on the $10\times10\,mm^2$ PTFE pieces (mass 0.017 g) cut from the sleeves was carried out by flame atomic absorbance spectroscopy (AAS) from a solution of conc. HCl/HNO_3 (aqua regia, 8.0 mL) against an Au standard/calibration from Au-$(NO_3)_3$. The AAS determined gold contents on the PTFE pieces increased with the concentration of the gold dispersion as follows: 1) on untreated PTFE (blank) a blind value of $0.2855\,mg\,L^{-1}$ or 0.0023 mg Au per PTFE piece was found and subsequently deducted from the measured Au values for the treated PTFE samples, 2) a 0.5 wt.% Au/IL dispersion gave $0.8235\,mg\,L^{-1}$ or 0.0066 mg Au per PTFE piece, 3) a 1 wt.% Au/IL dispersion gave $9.1925\,mg\,L^{-1}$ or 0.0735 mg per PTFE piece and 4) a 1.5 wt.% Au/IL gave $25.515\,mg\,L^{-1}$ or 0.2041 mg Au per PTFE piece.

Gold nanoparticle syntheses in ILs:

By thermal decomposition: Thermal decompositions were carried out under argon in a glass vessel which was connected to an oil bubbler. In a typical experiment Au(CO)Cl (0.040 g, 0.154 mmol) was dissolved/dispersed (during ≈1 h) under argon at room temperature in the presence of *n*-butylimidazole (1.5 equiv, 0.231 mmol) in the ionic liquid (3.0 g). The solution was slowly heated to 230 °C for 18 h under mechanical stirring. The decomposition process gave a dispersion with gold (0.03 g, 1 wt.% Au-NP in IL). During the decomposition process, a white haze of *n*-butylimidazolium chloride is formed. After cooling to room temperature under argon, a white-yellow precipitate (of *n*-butylimidazolium chloride in the below) was obtained and an aliquot of the ionic liquid was collected under argon atmosphere for in situ TEM/HRTEM, TED and dynamic light scattering (DLS) characterization. The white-yellow precipitate was collected by centrifugation (13200 rpm for 5 min) and decanting the supernatant Au/IL dispersion. The precipitate was washed twice with $CHCl_3$ (2 mL) and dried for several days under high vacuum. The dried white-yellow precipitate could be characterized as *n*-butylimidazolium chloride. Elemental analysis calcd (%): C 52.34, H 8.16, N 17.44; found C 52.69, H 8.28, N 17.56. ^{1}H NMR (200 MHz, $(CD_3)_2CO$, 20 °C, TMS as internal standard): δ = 9.02 (br, 1H; Aryl-*N*-CH-N), 8.6 (vbr, 1H; Aryl-NH), 7.67 (t, J = 1.5, 1H; Aryl-*N*-CH), 7.49 (t, J = 1.5, 1H; Aryl-*N*-CH), 4.4 (t, J = 7.3, 2H; NCH_2), 1.97 (m, J = 7.4, 2H; CH_2), 1,41 (m, J = 7.4, 2H; CH_2), 0.98 ppm (t, J = 7.4, 3H; CH_3) (see Figure S36 in the Supporting Information).

By photolysis: Photolytic decomposition of a solution/suspension of Au(CO)Cl (0.030 g, 0.115 mmol) in $BMIm^+BF_4^-$ (2.0 g) was carried out in a Kürner UV 1000 reactor from Kürner-Analysentechnik in quartz tubes for 1 min under argon using a Hg-UV lamp (1000 W) in the range between 200 and 450 nm to give a dispersion with of gold (0.020 g, ≈1 wt.% Au-NP in IL).

By microwave radiation: The microwave decomposition of a solution/suspension of Au(CO)Cl (0.030 g, 0.115 mmol) in $BMIm^+BF_4^-$ (2.0 g) was carried out in a CEM Discovery Microwave in a glass tube for 3 min at 10 W (250 °C) under argon without stirring to give a dispersion with gold (0.020 g, ≈1 wt.% Au-NP in IL).

Au-NP surface functionalization: Post synthetic surface functionalization of the dispersed gold nanoparticles in ILs was done by treating the 1wt.% Au-NP/IL dispersion with an excess of different organic thiol ligands. The volume ratio of the neat thiol liquid to the IL liquid was 5:1. The thiolated Au nanoparticles were collected under centrifugation (13200 rpm for 5 min) and then washed twice with a 20% (v/v) water–methanol mixture (2 mL) in an ultrasonic re-dispersion–centrifugation process. This process was repeated with 2 mL methanol (p.a.) to remove unbound thiol ligands.

Au-NP deposition on PTFE: It is also possible to carry out the above gold nanoparticle syntheses in ILs in the presence of a piece of PTFE for in situ Au-NP deposition onto PTFE. By adding a piece of PTFE to the thermal, photolysis, or microwave decomposition process the in situ gold deposition onto PTFE was obtained as a purple-red thin film.

Post synthetic photolytic deposition of a $10\times10\,mm^2$ PTFE piece with pre-synthesized Au-NPs from $BMIm^+BF_4^-$ were carried out in a Kürner UV 1000 reactor from Kürner-Analysentechnik in quartz tubes for 1 min under argon using a Hg-UV lamp (1000 W) in the range between 200 and 450 nm. Before UV irradiation, the PTFE pieces were dipped for 5 min into the pre-synthesized Au/IL dispersion (from thermal decomposition), then placed into quartz tubes without washing and irradiated.

Computational methods: The Kohn–Sham DFT calculations where performed with the program package GPAW.[74] The projector augmented wave method[73] was used and the smooth wave functions were represented on uniform real space grids. This approach provides a single convergence parameter, the grid-spacing, to control the accuracy of discretization. Similar techniques were successfully applied to gold clusters interactions with organic molecules[65,66,75,76] and ionic metal oxide surfaces.[71,78] The calculations were carefully tested for numerical convergence and found converge at a grid-spacing of 0.18 Å. The exchange-correlation energy was approximated in a generalized gradient approximation (GGA) as proposed by Perdew, Burke and Ernzerhof (PBE).[72] The results were cross-checked using the *meta*-GGA functional as proposed by Tao, Perdew, Staroverov and Scuseria.[89] No qualitative difference in the BE behavior by changing the PBE to the TPSS was observed (see also Figure S39 in the Supporting Information) and the absolute differences were found to be smaller than 0.08 eV in every case. Structures containing an even number of gold atoms were treated as spin-unpolarized, whereas structures containing an odd number of gold atoms were treated as spin-polarized calculations. The adducts of clusters connected to the ions or free bases were geometry optimized without symmetry restrictions. The structures were considered to be relaxed if the forces fell below $0.05\,eV\,Å^{-1}$. The charge analysis was performed using the Bader method.[90]

Acknowledgements

We thank Dr. T. J. S. Schubert from IoLiTec (Ionic Liquids Technologies GmbH, Denzlingen, Germany) for the donation of the ionic liquids. We also want to thank Dr. habil Schneider, Dr. Niranjan Ramgir, Dr. H. Müller-Sigmund, Dr. Peter Jankes, for their help and measurements. L. Hussein thanks the Deutsche Forschungsgemeinschaft (DFG) within the Graduiertenkolleg GR 1322, "Micro Energy Harvesting" for financial support. The project was partially funded by DFG grant JA466/17-1 and the University of Freiburg (Funktionelle metallhaltige Nanopartikel). M. Walter thanks the DFG priority program 1153 and the "black-forest grid" (BFG) for providing the computational resources.

[1] a) G. J. Hutchings, M. Haruta, *Appl. Catal.* **2005**, *291*, 1–261; b) M. Haruta, *Nature* **2005**, *437*, 1098–1099.
[2] V. Myroshnychenko, J. Rodríguez-Fernández, I. Pastoriza-Santos, A. M. Funston, C. Novo, P. Mulvaney, L. M. Liz-Marzán, F. J. García de Abajo, *Chem. Soc. Rev.* **2008**, *37*, 1792–1805.
[3] V. I. Pârvulescu, C. Hardacre, *Chem. Rev.* **2007**, *107*, 2615–2665.
[4] R. Elghanian, J. J. Storhoff, R. C. Mucic, R. L. Letsinger, C. A. Mirkin, *Science* **1997**, *277*, 1078–1081.
[5] a) J. A. Alonso, *Chem. Rev.* **2000**, *100*, 637–678; b) J. Blackman, *Metallic Nanoparticles*, Elsevier, Amsterdam, **2009**, pp. 113–141.
[6] C. Lee, Y. Kang, K. Lee, S. R. Kim, D.-J. Won, J. S. Noh, H. K. Shin, C. K. Song, Y. S. Kwon, H.-M. So, J. Kim, *Curr. Appl. Phys.* **2002**, *2*, 39–45.
[7] a) M. Faraday, *Philos. Trans. R. Soc. London* **1857**, *147*, 145–181; b) R. Zsigmondy, P. A. Thiessen, *Das Kolloide Gold*, Akademische Verlagsgesellschaft, Leipzig, **1925**, pp. 22–94.
[8] G. J. Hutchings, M. Brust, H. Schmidbaur, *Chem. Soc. Rev.* **2008**, *37*, 1759–1765.
[9] P. Wasserscheid, T. Welton, *Ionic Liquids in Synthesis, Vol. 1*, 2nd ed., Wiley-VCH, Weinheim, **2007**, pp. 325–350.
[10] J. Turkevich, P. C. Stevenson, J. Hillier, *Discuss. Faraday Soc.* **1951**, *11*, 55–75.

[11] G. Frens, *Nature* **1973**, *241*, 20–22.
[12] Y. Mastai, A. Gedanken, *Chemistry of Nanomaterials, Vol. 1* (Eds.: C. N. R. Rao, A. Müller, A. K. Cheetham), Wiley-VCH, Weinheim **2004** pp. 113–200.
[13] A. H. Lu, E. L. Salabas, F. Schüth, *Angew. Chem.* **2007**, *119*, 1242–1266; *Angew. Chem. Int. Ed.* **2007**, *46*, 1222–1244.
[14] A. Gedanken, *Ultrason. Sonochem.* **2004**, *11*, 47–55.
[15] C. N. R. Rao, S. R. C. Vivekchand, K. Biwas, A. Govindaraj, *Dalton Trans.* **2007**, 3728–3749.
[16] D. Mahajan, E. T. Papish, K. Pandya, *Ultrason. Sonochem.* **2004**, *11*, 385–392.
[17] J. Park, J. Joo, S. G. Kwon, Y. Jang, T. Hyeon, *Angew. Chem.* **2007**, *119*, 4714–4745; *Angew. Chem. Int. Ed.* **2007**, *46*, 4630–4660.
[18] A. Taubert, Z. Li, *Dalton Trans.* **2007**, 723–727.
[19] J. Dupont, *J. Braz. Chem. Soc.* **2004**, *15*, 341–350.
[20] C. S. Consorti, P. A. Z. Suarez, R. F. de Souza, R. A. Burrow, D. H. Farrar, A. J. Lough, W. Loh, L. H. M. da Silva, J. Dupont, *J. Phys. Chem. B* **2005**, *109*, 4341–4349.
[21] J. Dupont, P. A. Z. Suarez, R. F. de Souza, R. A. Burrow, J. P. Kintzinger, *Chem. Eur. J.* **2000**, *6*, 2377–2381.
[22] E. J. W. Verwey, J. T. G. Overbeek, *Theory of the Stability of Lyophobic Colloids*, 2nd ed., Dover Publications Mineola, **1999**, pp. 1–218.
[23] B. W. Ninham, *Adv. Colloid Interface Sci.*. **1999**, *83*, 111–136.
[24] a) G. A. Ozin, A. C. Arsenault, L. Cademartiri, *Nanochemistry*, 2nd ed., RSC, Cambridge, **2009**, pp. 335–428; b) G. Schmidt, *Nanoparticles*, Wiley-VCH, Weinheim, **2004**, pp. 185–238; c) F. Caruso, *Colloids and Colloid Assemblies*, Wiley-VCH, Weinheim, **2004**, pp. 96–119.
[25] D. Astruc, F. Lu, J. R. Aranzaes, *Angew. Chem.* **2005**, *117*, 8062–8083; *Angew. Chem. Int. Ed.* **2005**, *44*, 7852–7872.
[26] M. Antonietti, D. Kuang, B. Smarly, Y. Zhou, *Angew. Chem.* **2004**, *116*, 5096–5100; *Angew. Chem. Int. Ed.* **2004**, *43*, 4988–4992.
[27] L. S. Ott, R. G. Finke, *Coord. Chem. Rev.* **2007**, *251*, 1075–1100.
[28] E. Redel, R. Thomann, C. Janiak, *Inorg. Chem.* **2008**, *47*, 14–16.
[29] a) T. Gutel, J. Garcia-Antón, K. Pelzer, K. Philippot, C. C. Santini, L. S. Ott, R. G. Finke, *Inorg. Chem.* **2006**, *45*, 8382–8393, b) L. S. Ott, R. G. Finke, *Inorg. Chem.* **2006**, *45*, 8382–8393.
[30] G. S. Fonseca, A. P. Umpierre, P. F. P. Fichtner, S. R. Teixeira, J. Dupont, *Chem. Eur. J.* **2003**, *9*, 3263–3269.
[31] Z. Li, A. Friedrich, A. Taubert, *J. Mater. Chem.* **2008**, *18*, 1008–1014.
[32] P. Migowski, G. Machado, L. M. Rossi, G. Machado, J. Morais, S. R. Teixeira, M. C. M. Alves, A. Traverse, J. Dupont, *Phys. Chem. Chem. Phys.* **2007**, *9*, 4814–4821.
[33] J. M. Zhu, Y. H. Shen, A. J. Xie, L. G. Qiu, Q. Zhang, X. Y. Zhang, *J. Phys. Chem. C* **2007**, *111*, 7629–7639.
[34] M. A. Firestone, M. L. Dietz, S. Seifert, S. Trasobares, D. J. Miller, N. J. Zaluzec, *Small* **2005**, *1*, 754–760.
[35] K. Peppler, M. Polleth, S. Meiss, M. Rohnke, J. Z. Janek, *Z. Phys. Chem. (Muenchen Ger.)* **2006**, *220*, 1507–1527.
[36] A. Safavi, N. Maleki, F. Tajabadi, E. Farjami, *Electrochem. Commun.* **2007**, *9*, 1963–1968.
[37] K. Kim, C. Lang, P. A. Kohl, *J. Electrochem. Soc.* **2005**, *152*, E9.
[38] E. Redel, R. Thomann, C. Janiak, *Chem. Commun.* **2008**, 1789–1791.
[39] J. Krämer, E. Redel, R. Thomann, C. Janiak, *Organometallics* **2008**, *27*, 1976–1978.
[40] E. Redel, J. Krämer, R. Thomann, C. Janiak, *J. Organomet. Chem* **2009**, *694*, 1069–1075.
[41] D. O. Silva, J. D. Scholten, M. A. Gelesky, S. R. Teixeira, A. C. B. Dos Santos, E. F. Souza-Aguiar, J. Dupont, *ChemSusChem* **2008**, *1*, 291–294.
[42] M. Scariot, D. O. Silva, J. D. Scholten, G. Machado, S. R. Teixeira, M. A. Novak, G. Ebeling, J. Dupont, *Angew. Chem.* **2008**, *120*, 9215–9218; *Angew. Chem. Int. Ed.* **2008**, *47*, 9075–9078.
[43] F. Endres, A. P. Abbott, D. R. MacFarlane, *Electrodeposition from Ionic Liquids*, Wiley-VCH, Weinheim, **2008**, pp. 83–166; F. Endres, A. P. Abbott, D. R. MacFarlane, *Electrodeposition from Ionic Liquids*, Wiley-VCH, Weinheim, **2008**, pp. 213–238, and references therein.
[44] A. F. Holleman, N. Wiberg, *Lehrbuch der Anorganischen Chemie*, 102nd ed., Walter de Gruyter, Berlin, **2007**, pp. 1481–1482.
[45] a) J. D. Scholten, G. Ebeling, J. Dupont, *Dalton Trans.* **2007**, 5554–5560; b) D. Astruc, *Nanoparticles and Catalysis*, Wiley, New York, **2007**, pp. 22–24; c) V. Caló, A. Nacci, A. Monopoli, S. Laera, N. Coffi, *J. Org. Chem.* **2003**, *68*, 2929; d) R. R. Deshmuhk, R. Rajagopal, K. V. Srinivasan, *Chem. Commun.* **2001**, 1544; e) L. Xu, W. Chen, J. Xiao, *Organometallics* **2000**, *19*, 1123.
[46] a) P. J. Barnard, M. V. Baker, S. J. Berners-Price, B. W. Skelton, A. H. White, *Dalton Trans.* **2004**, 1038–1047; b) V. J. Catalano, A. L. Moore, *Inorg. Chem.* **2005**, *44*, 6558–6566; c) V. J. Catalano, A. O. Etogo, *Inorg. Chem.* **2007**, *46*, 5608–5615.
[47] P. Dash, R. W. J. Scott, *Chem. Commun.* **2009**, 812–814.
[48] H. Häkkinen, *Chem. Soc. Rev.* **2008**, *37*, 1847–1859.
[49] J. P. Tierney, P. Lidström, *Microwave Assisted Organic Synthesis*, Blackwell, New York, **2005**, pp. 20; J. P. Tierney, P. Lidström, *Microwave Assisted Organic Synthesis*, Blackwell, New York, **2005**, pp. 140; C. J. Coleman, *J. Austral. Math. Soc. Ser. B* **1991**, *33*, 1–8.
[50] I. Krossing, J. M. Slattery, *Z. Phys. Chem. (Muenchen Ger.)* **2006**, *220*, 1343–1359.
[51] A. N. Shipway, E. Katz, I. Willner, *ChemPhysChem* **2000**, *1*, 18–52.
[52] T. Cassagneau, J. H. Fendler, *J. Phys. Chem. B* **1999**, *103*, 1789–1793.
[53] C. D. Keating, K. K. Kovaleski, M. J. Natan, *J. Phys. Chem. B* **1998**, *102*, 9404–9413.
[54] E. Redel, J. Krämer, R. Thomann, C. Janiak, *GIT Lab. J.* **2008**, *04*, 400–404.
[55] T. J. Gannon, G. Law, R. P. Watson, A. J. Carmichael, K. R. Seddon, *Langmuir* **1999**, *15*, 8429–8434.
[56] G. Law, R. P. Watson, A. J. Carmichael, K. R. Seddon, *Phys. Chem. Chem. Phys.* **2001**, *3*, 2879–2885.
[57] J. N. Canongia Lopes, M. F. C. Gomes, A. A. H. Pádua, *J. Phys. Chem. B* **2006**, *110*, 16816–16818.
[58] J. N. Canongia Lopes, A. A. H. Pádua, *J. Phys. Chem. B* **2006**, *110*, 3330–3335.
[59] C. S. Weisbecker, M. V. Merritt, G. M. Whitesides, *Langmuir* **1996**, *12*, 3763–3772.
[60] S. Chen, K. Kimura, *Chem. Lett.* **1999**, 1169–1170.
[61] STOE WinXPow version 1.10, data base, STOE & Cie GmbH, Darmstadt, Germany, **2002**.
[62] O. P. Khatri, K. Adachi, K. Murase, K-I. Okazaki, T. Torimoto, N. Tanaka, S. Kuwabata, H. Sugimura, *Langmuir* **2008**, *24*, 7785–7792.
[63] Y. Shichibu, Y. Negishi, T. Tsukuda, T. Teranishi, *J. Am. Chem. Soc.* **2005**, *127*, 13464–13465.
[64] R. Balasubramanian, R. Guo, A. J. Mills, Royce W. Murray, *J. Am. Chem. Soc.* **2005**, *127*, 8126–8132.
[65] M. Walter, J. Akola, O. Lopez-Acevedo, P. D. Jadzinsky, G. Calero, C. J. Ackerson, R. L Whetten, H. Grönbeck, H. Häkkinen, *Proc. Natl. Acad. Sci. USA* **2008**, *105*, 9157–9162.
[66] J. Akola, M. Walter, R. L. Whetten, H. Häkkinen, H. Grönbeck, *J. Am. Chem. Soc.* **2008**, *130*, 3756–3757.
[67] P. Dutta, S. Pal, M. S. Seehra, M. Anand, C. B. Roberts, *Appl. Phys. Lett.* **2007**, *90*, 213102–213103.
[68] A. P. Umpierre, G. Machado, G. H. Fechner, J. Morais, J. Dupont, *Adv. Synth. Catal.* **2005**, *347*, 1404–1412.
[69] G. Machado, J. D. Scholten, T. de Vargas, S. R. Teixeira, L. H. Ronchi, J. Dupont, *Int. J. Nanotechnol.* **2007**, *4*, 541–563.
[70] S. Özkar, R. G. Finke, *J. Am. Chem. Soc.* **2002**, *124*, 5796–5810.
[71] a) Z. Wang, Q. Zhang, D. Kuehner, A. Ivasaka, L. Niu, *Green Chem.* **2008**, *10*, 907–909; b) Ki-Sub Kim, D. Demberelnyamba, H. Lee, *Langmuir* **2004**, *20*, 556–560.
[72] J. P. Perdew, K. Burke, M. Ernzerhof, *Phys. Rev. Lett.* **1996**, *77*, 3865–3868.
[73] P. E. Blöchl, *Phys. Rev. B* **1994**, *50*, 17953–17979.
[74] J. J. Mortensen, L. B. Hansen, K. W. Jacobsen, *Phys. Rev. B* **2005**, *71*, 035109.

[75] H. Häkkinen, M. Walter, H. Grönbeck, *J. Phys. Chem. B* **2006**, *110*, 9927–9931.
[76] H. Grönbeck, M. Walter, H. Häkkinen, *J. Am. Chem. Soc.* **2006**, *128*, 10268–10275.
[77] M. Walter, H. Häkkinen, *Phys. Rev. B* **2005**, *72*, 205440.
[78] M. Walter, P. Frondelius, K. Honkala, H. Häkkinen, *Phys. Rev. Lett.* **2007**, *99*, 096102.
[79] C. Bauschlicher, S. R. Langhoff, H. Patridge, *J. Chem. Phys.* **1989**, *91*, 2412.
[80] H. Häkkinen, U. Landmann, *Phys. Rev. B* **2000**, *62*, R2287–R2290.
[81] P. Gruene, D. M. Rayner, B. Redlich, A. F. G. Van der Meer, J. T. Lyon, G. Meijer, A. Fielicke, *Science* **2008**, *321*, 674–676.
[82] C. M. Aikens, G. C. Schatz, *J. Phys. Chem. A* **2006**, *110*, 13317–13324.
[83] H. Häkkinen, B. Yoon, U. Landmann, X. Li, H. J. Zhai, L. S. Wang, *J. Phys. Chem. A* **2003**, *107*, 6168–6175.
[84] T. A. Baker, C. M. Friend, E. Kaxiras, *J. Am. Chem. Soc.* **2008**, *130*, 3720–3721.
[85] F. Endres, S. Z. El Abedin, *Phys. Chem. Chem. Phys.* **2006**, *8*, 2101–2116.
[86] P. Wasserscheid, T. Welton, *Ionic Liquids in Synthesis, Vol. 1* 2nd ed., Wiley-VCH, Weinheim, **2007**, pp. 32–61.
[87] R. P. Swatloski, J. D. Holbrey, R. D. Rogers, *Green Chem.* **2003**, *5*, 361–363.
[88] G. A. Baker, S. N. Baker, *Aust. J. Chem.* **2005**, *58*, 174–177.
[89] J. Tao, J. P. Perdew, V. N. Staroverov, G. E. Scuseria, *Phys. Rev. Lett.* **2008**, *100*, 206405.
[90] G. Henkelman, A. Arnaldson, H. Jonsson, *Comput. Mater. Sci.* **2006**, *36*, 354–360.

Received: February 4, 2009
Revised: May 5, 2009
Published online: August 20, 2009

